IOP Publishing Journal of Physics D: Applied Physics
J. Phys. D: Appl. Phys. **40** (2007) 6953–6968 doi:10.1088/0022-3727/40/22/016

Continuous processing of polymers in repetitively pulsed atmospheric pressure discharges with moving surfaces and gas flow

Ananth N Bhoj[1,3] **and Mark J Kushner**[2,4]

[1] Department of Chemical and Biomolecular Engineering, University of Illinois, Urbana, IL 61801, USA
[2] Department of Electrical and Computer Engineering, Iowa State University, Ames, IA 50011, USA

E-mail: ananth.bhoj@novellus.com and mjk@iastate.edu

Received 5 July 2007, in final form 5 August 2007
Published 2 November 2007
Online at stacks.iop.org/JPhysD/40/6953

Abstract
Atmospheric pressure corona discharges are industrially employed to treat large areas of commodity polymer sheets by creating new surface functional groups. The most common processes use oxygen containing discharges to affix oxygen to hydrocarbon polymers, thereby increasing their surface energy and wettability. The process is typically continuous and is carried out in a web configuration with film speeds of tens to hundreds of cm s^{-1}. The densities and relative abundances of functional groups depend on the gas composition, gas flow rate and residence time of the polymer in the discharge zone which ultimately determine the magnitude and mole fractions of reactive fluxes to the surface. In this paper, results are discussed from a two-dimensional computational investigation of the atmospheric pressure plasma functionalization of a moving polypropylene sheet in repetitively pulsed $He/O_2/H_2O$ discharges. O and OH typically initiate surface processing by hydrogen abstraction. These species are regenerated during every plasma pulse but are also largely consumed during the inter-pulse period. Longer-lived species such as O_3 accumulate over many pulses and convect downstream with the gas flow. Optimizing the interplay between local rapid reactions, such as H abstraction which occurs dominantly in the discharge zone, and non-local slower processes, such as surface–surface reactions, may enable the customization of the relative abundance of surface functional groups.

1. Introduction

Plasma discharges generated at atmospheric pressure are often employed to functionalize the surfaces of polymers to improve their wettability [1]. These plasma sources have the advantages of short treatment times, room temperature operation and dispensing with the vacuum equipment required for low pressure processing. Typical plasma sources are atmospheric pressure corona discharges in a dielectric barrier configuration operating at a few kHz to tens of kHz with electrode separations of few mm [2]. Such discharges are used to inexpensively

[3] Present address: Novellus Systems, Inc., 3011 N. 1st St, San Jose, CA 95134, USA.
[4] Author to whom any correspondence should be addressed.

(a few cents per m^2) functionalize the surfaces of large areas of commodity polymer films (e.g. polypropylene) in a web configuration using an apparatus analogous to a printing press (see figure 1). In web processing, the film is continuously moved through the discharge at speeds of up to many metres per second with residence times of tens of microseconds to a few milliseconds in the discharge. In high volume industrial processing, the polymer sheets may be moved through multiple stages of treatment, one or more of which may involve plasma treatment. Gas flow is often employed to maintain constant pressure or to transport reactive species generated in the discharge over a larger surface area to reduce inhomogeneities in surface treatment [3, 4].

The most often applied process in web treatment of polymers is increasing the surface energy of otherwise hydrophobic hydrocarbon polymer films to increase their wettability and so make them more hydrophilic [5]. This is accomplished by fixing O atoms to the surface by first creating active sites on the polymer, usually by abstracting surface resident hydrogen, followed by reaction with oxygen containing species either created by the plasma or contained in the feedstock gas. For example, affixing O atoms to a hydrocarbon polymer in an atmospheric pressure corona discharge in air can occur by O atom abstraction of H from the hydrocarbon backbone creating an alkyl site, followed by passivation with O_2 to create a peroxy site [6, 7].

The processes occurring during such treatment include breakdown of the gas upon application of a voltage pulse on timescales of ns, gas phase heavy particle reaction kinetics on timescales of μs and convective and diffusive transport of heavy species and surface reaction kinetics on timescales of ms [8, 9]. Previous investigators have computationally investigated these processes using one-dimensional (1D) and two-dimensional (2D) models to describe the dynamics of high pressure breakdown, propagation of streamers and plasma chemistry. For instance, Wang and Kunhardt [10] developed models to describe the space–time evolution of streamer fronts to elucidate the properties of positive and negative streamers. Vitello *et al* [11] used results from 2D and three-dimensional (3D) simulations of streamer dynamics in nitrogen to demonstrate the different phases of streamer evolution. Kulikovsky [12] used 2D simulations to highlight the role of photoionization in the propagation of positive corona discharges in air. Models that also account for gas phase heavy particle reaction kinetics on longer timescales were developed for applications such as ozone generation [13, 14], excimer production [15, 16] and remediation of toxic gases [17, 18].

Models for surface reaction kinetics during plasma treatment of polymers are usually more hierarchical due to there being fewer definitive and validated reaction mechanisms for plasma-surface interactions. For example, Clark and Dilks [19, 20] investigated polymer surface modification in low pressure radio frequency glow discharges using Ar, H_2 and He/O_2. The XPS data was analysed using energy transfer models to postulate roles for the active plasma species. Normand *et al* [21] used analytical transport equations to develop a reaction mechanism for the treatment of polypropylene in O_2 microwave discharges and concluded that O atoms initiate surface reaction pathways. More recently, an integrated zero-dimensional (0D) plasma chemistry–surface kinetics model was used to investigate production of reactive species in humid air and a surface reaction mechanism was developed for the treatment of polypropylene [22]. Statistical theory and design of experiments approaches have also been used to build regressive models [23, 24] capable of predicting changes in water contact angle and O atom content of polymer films treated in dielectric barrier discharges.

In this paper, results are discussed from a 2D computational investigation of the functionalization of the surface of moving polypropylene sheets by a repetitively pulsed atmospheric pressure corona discharge. The model spans time scales of ns to tens of ms to address the plasma dynamics, gas phase and surface chemistry and forced gas flow, as well as the consequences of the moving surface of the polymer web. Single and repetitively pulsed discharges in $He/O_2/H_2O$ mixtures are discussed. Since gas phase radicals are transported, either diffusively or by forced gas flow, to the moving polymer and react to produce new surface and gas phase species, the interaction between the flow field, film speed and the surface and gas phase chemical kinetics ultimately determine the density of surface functional groups.

We found that forced gas flow alters the relative flux of radicals generated by the discharges, such as O and O_3, along the surface of the polymer. As such, a combination of forced gas flow and speed of the moving polymer sheet can be used to customize the functional groups produced on the surface. Reactive species such as O and OH are regenerated during every discharge pulse but are consumed by reactions before they are significantly transported by the flow. Their influence on surface properties is largely in the immediate vicinity of the electrodes. Longer-lived species such as O_3 accumulate over many pulses and are transported downstream by the forced flow, thereby extending their influence on surface properties. The surface properties are also controllable through choice of discharge geometry. In configurations where discharges are arrayed along the direction of sheet motion, sites receive renewed fluxes of short lived radicals (e.g. O and OH) as a given site on the surface passes through each discharge. This ultimately leads to higher surface coverage of functional groups.

The model and reaction mechanisms used in this investigation are described in sections 2 and 3 followed by a discussion of functionalization of stationary and moving polymer sheets in the absence of forced gas flow in section 4. The consequences of forced gas flow on functionalization are discussed in section 5 and of alternate discharge geometries in section 6. Our concluding remarks are presented in section 7.

2. Description of the model

The 2D modelling platform used in this investigation, *nonPDPSIM*, has 3 major modules addressing plasma dynamics, fluid dynamics and surface kinetics. *nonPDPSIM* is implemented on an unstructured mesh, as described in detail elsewhere, to enable resolution of a large dynamic range in space [25].

Briefly, the plasma dynamics module is used to solve Poisson's equation for the electric potential simultaneously with the multi-fluid charged and neutral species conservation

equations on an unstructured mesh. The equations solved for charged species are

$$-\nabla\cdot\varepsilon\nabla\Phi=\sum_j n_j q_j+\rho_S, \tag{1}$$

$$\frac{\partial N_i}{\partial t}=(-\nabla\cdot\vec{\phi}_i+S_i), \tag{2}$$

$$\frac{\partial\rho_S}{\partial t}=\left(\sum_i -\nabla\cdot(q_i\vec{\phi}_i(1+\gamma_i))+\nabla\cdot(\sigma\nabla\Phi)\right), \tag{3}$$

where ε, Φ, ρ_s, N, ϕ, γ, σ, S and q refer to the permittivity, electric potential, surface charge density, charged species number density, species flux, secondary electron emission coefficient, conductivity of solid materials, source terms and elementary charge, respectively. Gain and loss terms due to electron impact ionization and excitation, heavy particle reactions, photoionization, secondary emission and surface reactions are included. The subscript denotes the identity of the species. Charged particle fluxes are provided by a modified Scharfetter–Gummel technique that accounts for entrainment of ions in the neutral flow field. The solution technique employs a Newton iteration method to implicitly and simultaneously integrate the finite-volume discretized forms of equations (1)–(3).

The multi-fluid continuity equations for neutral densities are solved in a time-spliced manner following the update of charged particle densities,

$$\frac{\mathrm{d}N_i}{\mathrm{d}t}=-\nabla\cdot\left(\vec{v}N_i-D_iN_\mathrm{T}\nabla\left(\frac{N_i}{N_\mathrm{T}}\right)\right)+S_\mathrm{Vi}+S_\mathrm{Si}, \tag{4}$$

where N_i is the density of species i, N_T is the total gas density, $\vec{v}$ is the species averaged advective velocity, D_i is the diffusion coefficient, S_Vi is the source function due to volumetric processes and S_Si is the source function due to surface processes.

The electron energy equation is integrated for average energy ε,

$$\frac{\mathrm{d}}{\mathrm{d}t}(n_\mathrm{e}\varepsilon)=q\vec{\phi}_\mathrm{e}\cdot\vec{E}-n_\mathrm{e}\sum_i N_ik_i\Delta\varepsilon_i-\nabla\cdot\left(\frac{5}{2}\varepsilon\vec{\phi}_\mathrm{e}-\lambda\nabla T_\mathrm{e}\right), \tag{5}$$

where T_e is the electron temperature defined as $(2\,\varepsilon/3)$, n_e is the electron density, k_i is the rate coefficient for collision process i with species having density N_i and energy loss $\Delta\varepsilon_i$, λ is the electron thermal conductivity and $\vec{\phi}_\mathrm{e}$ is the electron flux.

The velocity flow field for the neutral gas, which is treated as a single fluid, is calculated using a newly developed incompressible flow option within the fluid dynamics model described in [25]. This option is implemented using an artificial compressibility [26, 27] technique in which the momentum equation is solved with a pseudo-continuity equation having pressure p acting as a relaxation parameter. This enforces the zero divergence criterion on the calculated velocity flow field v. The equations solved are

$$\frac{\partial p}{\partial t}+\beta^2(\nabla\cdot\vec{v})=0, \tag{6a}$$

$$\frac{\partial\rho\vec{v}}{\partial t}=-\nabla\cdot(\rho\vec{v}\vec{v})+\left(-\nabla p+\nabla\cdot\left(\mu\left(\nabla\vec{v}+(\nabla\vec{v})^\mathrm{T}-\frac{2}{3}(\nabla\vec{v})\cdot I\right)\right)-\rho\vec{g}+\vec{S}_\mathrm{M}\right), \tag{6b}$$

$$\rho c_p\frac{\partial T_\mathrm{g}}{\partial t}=-c_pT_\mathrm{g}\frac{\partial\rho}{\partial t}-(\nabla\cdot(\rho c_pT_\mathrm{g}\vec{v}-\kappa\nabla T_\mathrm{g}))+S_\mathrm{E}+S_\mathrm{T}, \tag{6c}$$

where β is a compressibility parameter between 0.5 and 2.0. In equations (6*a*)–(6*c*), ρ is the gas mass density, g is the gravitational constant, c_p is the heat capacity, μ is the viscosity, κ is the thermal conductivity and T_g is the gas temperature. S_M and S_E represent contributions to the momentum and energy due to the interaction of charged particle fluxes with the electrostatic field [28]. S_T includes source terms for viscous dissipation and the change in enthalpy due to chemical and electron impact reactions. The technique used to solve the system of equations (6*a*)–(6*c*) is similar to the method described in [25]. Using the artificial compressibility technique, the density of the gas is a function of only local gas temperature and is obtained from the ideal gas law.

The surface kinetics module (SKM) consists of a modified surface site–balance algorithm implemented at the nodes of specified materials that border the plasma domain. The method is functionally the same as that described in [29]. The SKM is implemented on computational nodes bordering the plasma identified as being polymer. The SKM accepts fluxes of gas phase species (neutrals, ions and electrons) and photons and applies a user-specified surface reaction mechanism to calculate the change in the area density of surface resident species. An outcome of the SKM is reactive sticking coefficients of gas phase species incident on the surface as used in the gas phase model. The reaction mechanism consists primarily of gas phase species reacting on the surface sites, but it also allows for photochemistry and surface sites reacting with each other.

The time rate of change of the surface coverage (sites per unit area), θ_j, of species j is

$$\left(\frac{\partial\theta_j}{\partial t}\right)=-\theta_j\left(\sum_i\phi_ik_{ij}+\sum_{lm}\theta_mp'_{jm}\right)+\sum_{i,m}\theta_m\phi_ip_{im}+\sum_{l,m}\theta_l\theta_mp'_{lm}, \tag{7}$$

where ϕ_i is the flux of gas phase species i (including photons), p_{ij} is the reaction probability between θ_j, and ϕ_i and p'_{ij} is the probability for reaction between surface species. The first two summations account for reactions with gas phase and surface species depleting θ_j. The second two summations account for its replenishment. The set of differential equations representing equation (7) were explicitly integrated in time. Outputs from the SKM include the fractional coverage of surface resident species and returning fractions for gas phase reactants and products as a result of the surface reactions. Initial conditions for the SKM consist of surface coverage of species found on the virgin surface.

The time required for the surface resident species to come into a steady state is long compared with the residence time of the polymer surface in the plasma zone. Untreated surface

sites move into the plasma zone (beneath the electrodes), are partially functionalized and move downstream where neutral radicals further treat the sites. As result, the physical motion of the web must be accounted for. To address these phenomena, the following technique was used.

The direction (e.g. entering from the left and exiting to the right) and linear speed of the polymer sheet are specified. The nodes in the mesh on the surface of the polymer are searched for and sequentially ordered from entrance to exit. (For purposes of discussion, assume that the sheet enters from the left and exits to the right.) A handoff time, Δt_H, is defined as the spacing of the surface mesh points divided by the translational speed of the surface. Every Δt_H the surface properties (e.g. the fractional surface coverage for each surface species, temperature and surface charge density) are translated between adjacent surface mesh points; the properties of a mesh point to the left are moved to the mesh point to its right. The left most mesh point (representing the input of the web to the computational domain) has fixed surface properties corresponding to untreated material. The properties of the rightmost surface mesh point translate out of the computational domain. Transfer of momentum from the moving film to the gas was not accounted for.

The plasma devices we modelled are typically operated at many hundreds of Hz to tens of kHz. A discharge pulse length of at most tens of ns is followed by an inter-pulse period of tens of μs to a few ms. Knowing that the plasma largely dissipates by electron recombination, attachment and ion–ion recombination on times short compared with the inter-pulse period, the following method was used to model the repetitively pulsed discharges.

Based on previous experience, a plasma period Δt_p is specified which is of sufficient length to allow the discharge to avalanche, evolve and extinguish. During Δt_p the equations for charged particle densities, electric potential, neutral and surface densities, and flow properties are integrated. After Δt_p, Poisson's equation is no longer solved, electric fields are set to zero and the remaining conservation equations are integrated without the limitation of the dielectric relaxation time. This continues for the remainder of the inter-pulse period. At the time for the next discharge pulse, voltage is applied to the electrode and gas phase charged particles densities are reinitialized to small but finite values in the vicinity of the tip of the electrode (see below) to initiate the next avalanche. All this occurs while translating the surface properties representing motion of the film every Δt_H. The process is repeated for a specified number of discharge pulses.

3. Reaction mechanisms

Many commercial corona discharge devices for functionalization of sheet polymers operate in room air. In previous studies [30] it was shown that the relative coverages of surface groups can be controlled through judicious choices of gas mixtures. As such, and based on previous experience, this investigation was performed using an atmospheric pressure $He/O_2/H_2O$ gas mixture. The full gas phase reaction mechanism is similar to that discussed in [22] with O containing species dominating the reaction chemistry. A few reactions particularly relevant to the functionalization of PP are discussed below.

In the reaction mechanism developed in [22], surface reactions on the polymer are initiated by H abstraction from the hydrocarbon backbone by O and OH as shown in table 1. These species are dominantly generated by electron impact dissociation of O_2 and H_2O in the gas phase:

$$e^- + O_2 \rightarrow O + O + e, \tag{8}$$

$$e^- + H_2O \rightarrow H + OH + e. \tag{9}$$

Three body reactions dominate the subsequent neutral reaction kinetics. O atoms are largely consumed by reactions with O_2 to form O_3. H reacts at slower rates with O_2 to form HO_2:

$$O + O_2 + M \rightarrow O_3 + M \quad (k = 6.9 \times 10^{-34} T_g^{-1.25}\ \mathrm{cm^6\ s^{-1}}), \tag{10}$$

$$H + O_2 + M \rightarrow HO_2 + M \quad (k = 6.1 \times 10^{-32} T_g^{-1.6}\ \mathrm{cm^6\ s^{-1}}), \tag{11}$$

where k is the rate coefficient and M is a third body.

There are no major gas phase consumption pathways for O_3 at the temperatures of interest (within tens of degrees of room temperature) and so O_3 tends to accumulate from pulse to pulse. O_3 does slowly react with H to form OH, with O to form O_2 and with OH to form HO_2:

$$H + O_3 \rightarrow OH + O_2$$
$$(k = 1.4 \times 10^{-10} \exp(-470/T_g)\ \mathrm{cm^3\ s^{-1}}), \tag{12}$$

$$O + O_3 \rightarrow O_2 + O_2$$
$$(k = 8 \times 10^{-12} \exp(-2060/T_g)\ \mathrm{cm^3\ s^{-1}}), \tag{13}$$

$$OH + O_3 \rightarrow HO_2 + O_2$$
$$(k = 1.9 \times 10^{-12} \exp(-1000/T_g)\ \mathrm{cm^3\ s^{-1}}). \tag{14}$$

HO_2 in turn slowly reacts with radicals such as O, H and OH forming other radicals or stable products. OH and O mutually react at slow rates to form H:

$$HO_2 + O \rightarrow OH + O_2$$
$$(k = 2.9 \times 10^{-11} \exp(-200/T_g)\ \mathrm{cm^3\ s^{-1}}), \tag{15}$$

$$HO_2 + OH \rightarrow H_2O + O_2 \quad (k = 8 \times 10^{-11}\ \mathrm{cm^3\ s^{-1}}), \tag{16}$$

$$HO_2 + H \rightarrow H_2O + O \quad (k = 2.4 \times 10^{-12}\ \mathrm{cm^3\ s^{-1}}), \tag{17}$$

$$O + OH \rightarrow H + O_2$$
$$(k = 2.3 \times 10^{-11} \exp(110/T_g)\ \mathrm{cm^3\ s^{-1}}). \tag{18}$$

The end result is that the dominant neutral radical fluxes to the surface which are responsible for the surface functionalization are O, O_3 and OH. Surface treatment occurs over multiple discharge pulses and inter-pulse periods.

The basis of surface reaction mechanism for functionalization of PP in oxygen containing plasmas is discussed in [22]. Our updated mechanism is listed in its entirety in table 1. Some of the salient features of the mechanism follow. In this discussion RH represents a hydrogen atom on the hydrocarbon backbone (R). The PP monomer, CH_2–CH–CH_3, contains primary, secondary and tertiary sites for the hydrogen atoms, with

Table 1. Surface reaction mechanism.

Surface species	
R_n–H	PP Backbone (n: 1 =tertiary, 2 =secondary, 3 =primary sites)
R_{ns}–H	Chain scission product
R_n–•	Alkyl
R_n–O•	Alkoxy
R_n–OO•	Peroxy
R_n–OOH	Hydroperoxy
HR_n=O	Carbonyl
•R_n=O	Carbonyl radical
R_n–OH	Alcohol
OH–R=O	Acid
•R=O	Crosslink

Reaction	Probability or rate constant[a]
Gas–surface reactions[b]	
$O + R_1–H \rightarrow OH + R_1•$	0.001
$O + R_2–H \rightarrow OH + R_2•$	0.0001
$O + R_3–H \rightarrow OH + R_3•$	0.00001
$O + R_1• \rightarrow R_1–O•$	0.1
$O + R_2• \rightarrow R_2–O•$	0.1
$O + R_3• \rightarrow HCHO + R_1•$	0.01
$O + HR_2=O \rightarrow OH + •R=O$	0.04
$O + •R=O \rightarrow CO_2 + R_1–H$	0.1
$O + •R=O \rightarrow CO_2 + R_2–H$	0.2
$O + •R=O \rightarrow CO_2 + R_3–H$	0.1
$O + R_1–OH \rightarrow R_1–O• + OH$	7.5×10^{-4}
$O + R_{1s}–H \rightarrow R_{1s}–O$	0.1
$O + R_{2s}–H \rightarrow R_{2s}–O$	0.1
$OH + R_1–H \rightarrow H_2O + R_1•$	0.1
$OH + R_2–H \rightarrow H_2O + R_2•$	0.05
$OH + R_3–H \rightarrow H_2O + R_3•$	0.012
$OH + R_2• \rightarrow R_2–OH$	1×10^{-5}
$OH + R_1• \rightarrow R_1–OH$	1×10^{-5}
$OH + R_3• \rightarrow R_3–OH$	1×10^{-5}
$OH + HR_2=O \rightarrow H_2O + •R=O$	0.4
$OH + •R=O \rightarrow OH–R=O$	0.12
$OH + R_1–OH \rightarrow R_1–O + H_2O$	0.0082
$OH + R_1–OO• \rightarrow R_1–OH + O_2$	1×10^{-5}
$OH + R_2–OO• \rightarrow R_2–OH + O_2$	1×10^{-5}
$OH + R_{1s}–H \rightarrow R_{1s}–OH$	1×10^{-5}
$OH + R_{2s}–H \rightarrow R_{2s}–OH$	1×10^{-5}
$O_2 + R_1• \rightarrow R_1–OO•$	0.001
$O_2 + R_2• \rightarrow R_2–OO•$	2.2×10^{-4}
$O_2 + R_3• \rightarrow R_3–OO•$	5×10^{-4}
$O_2 + R_{1s}–H \rightarrow R_{1s}–OO•$	0.001
$O_2 + R_{2s}–H \rightarrow R_{2s}$	0.001
$O_3 + R_1• \rightarrow R_1–O• + O_2$	1.0
$O_3 + R_2• \rightarrow R_2–O• + O_2$	0.5
$O_3 + R_3• \rightarrow R_3–O• + O_2$	0.5
$HO_2 + R_1–OO• \rightarrow R_1–OOH + O_2$	1×10^{-5}
$HO_2 + R_2–OO• \rightarrow R_2–OOH + O_2$	1×10^{-5}
Surface–surface reactions[b]	
$R_1–O• + R_2–H \rightarrow HR_1=O + R_{1s}–H$	3.2×10^{-14}
$R_1–O• + R_2–H \rightarrow R_1–OH + R_2•$	8×10^{-14}
$R_1–O• + R_3–H \rightarrow R_1–OH + R_3•$	8×10^{-14}
$R_1–O• + R_1–OOH \rightarrow R_1–OH + R_1–OO•$	1×10^{-20}
$R_1–O• + R_2–OOH \rightarrow R_1–OH + R_2–OO•$	1×10^{-20}
$R_2–O• + R_1–H \rightarrow HR_2=O + R_{2s}–H$	9.4×10^{-13}
$R_2–O• + R_1–H \rightarrow R_2–OH + R_1•$	3×10^{-14}
$R_2–O• + R_3–H \rightarrow HR_2=O + R_{2s}–H$	9.4×10^{-13}
$R_2–O• + R_3–H \rightarrow R_2–OH + R_3•$	3×10^{-14}
$R_2–O• + R_1–OOH \rightarrow R_2–OH + R_1–OO•$	1×10^{-20}
$R_2–O• + R_2–OOH \rightarrow R_2–OH + R_2–OO•$	1×10^{-20}
$R_1–OO• + R_1–H \rightarrow R_1–OOH + R_1•$	5.5×10^{-16}
$R_2–OO• + R_1–H \rightarrow R_2–OOH + R_1•$	5.5×10^{-16}
$R_3–OO• + R_1–H \rightarrow R_3–OOH + R_1•$	5.5×10^{-16}
$R_{1s}–O + R_3–H \rightarrow HCHO + R_{2s}–H$	5.5×10^{-16}
$R_{2s}–O + R_2–H \rightarrow CH_3CHO + R_{1s}–H$	5.5×10^{-16}
$R_{1s}–OO• + R_1–H \rightarrow R_{1s}–OOH + R_1•$	5.5×10^{-16}
$R_{2s}–OO• + R_2–H \rightarrow R_{2s}–OOH + R_2•$	5.5×10^{-16}
Photon-surface interactions[c]	
$h\nu + R_1–H \rightarrow R_1• + H$	0.01
$h\nu + R_2–H \rightarrow R_2• + H$	0.01
$h\nu + R_3–H \rightarrow R_3• + H$	0.01
$h\nu + R_1–H \rightarrow R_2• + CH_3$	2×10^{-4}
$h\nu + R_1–H \rightarrow$ •R–CH–CH–R• + H_2	0.08
$h\nu + R_1–H \rightarrow R_{1s}–H + R_{2s}–H$	0.04
$h\nu + R_2–H \rightarrow R_{1s}–H + R_{2s}–H$	0.04
Cross linking[d]	
•R–CH–CH–R• + $R_1–H \rightarrow$ R=R	1×10^{-15}
•R–CH–CH–R• + $R_2–H \rightarrow$ R=R	1×10^{-15}
•R–CH–CH–R• + $R_3–H \rightarrow$ R=R	1×10^{-15}
$R_{1s}–H + R_{1s}–H \rightarrow$ R=R	1×10^{-15}
$R_{1s}–H + R_{2s}–H \rightarrow$ R=R	1×10^{-15}
$R_{2s}–H + R_{2s}–H \rightarrow$ R=R	1×10^{-15}
Ion bombardment cleaving C–H bonds[e]	
$O^+ + R_1–H \rightarrow R_1• + OH$	0.001
$O^+ + R_2–H \rightarrow R_2• + OH$	0.001
$O^+ + R_3–H \rightarrow R_3• + OH$	0.001
$O_2^+ + R_1–H \rightarrow R_1• + O_2 + H$	0.001
$O_2^+ + R_2–H \rightarrow R_2• + O_2 + H$	0.001
$O_2^+ + R_3–H \rightarrow R_3• + O_2 + H$	0.001
$He^+ + R_1–H \rightarrow R_1• + He + H$	0.001
$He^+ + R_2–H \rightarrow R_2• + He + H$	0.001
$He^+ + R_3–H \rightarrow R_3• + He + H$	0.001

[a] Rate constants for gas–surface, photon–surface and ion–surface reactions are probabilities. For surface–surface reactions, rate constants are in units of $cm^2\ s^{-1}$. First order reactions have rate constants of s^{-1}.
[b] Basis of rate coefficients are obtained from [22] with modifications discussed in text to better align with experimental observations.
[c] Rate coefficients scaled from [33, 36, 37]. See also discussion in text.
[d] Reactions obtained from [38–40] with rate coefficients estimated.
[e] Rate coefficients estimated from [32].

varying reactivities (tertiary the highest, primary the lowest). Although these sites are differentiated in table 1, in the discussion that follows, RH generically represents all three sites and the probability indicated is for the tertiary sites.

Functionalization of PP comes about by initiation, propagation and termination reaction pathways, similar to free radical gas phase chemistry. The initiation steps typically consists of abstraction of H from an RH site by a gas phase species:

$$RH + O \rightarrow R• + OH, \qquad p = 10^{-3}, \tag{19}$$

$$RH + OH \rightarrow R• + H_2O, \qquad p = 0.1. \tag{20}$$

where p is the reaction probability for the tertiary site. The resulting alkyl (R•) radicals react with O and O_3 to form alkoxy (R–O•) groups,

$$R• + O \rightarrow R–O• \qquad p = 0.1, \tag{21}$$

$$R• + O_3 \rightarrow R–O• + O_2 \qquad p = 1.0. \tag{22}$$

The reaction of R• radicals with O_2 to form peroxy (R–OO•) groups has a lower probability,

$$R• + O_2 \rightarrow R–OO• \qquad p = 10^{-3}. \tag{23}$$

The density of O_2 is usually much higher than the radicals and so the absolute rate at which this reaction proceeds is large.

Reactions between surface species can also occur (with the rate coefficients having units of $cm^2\,s^{-1}$ which are subsequently scaled by the total density of surface sites). For instance, rapid abstraction of H atoms from surrounding RH sites by alkoxy (R–O•) sites produces alcohol (R–OH) groups:

$$\text{R–O•} + \text{RH} \rightarrow \text{R–OH} + \text{R•} \quad p = 8 \times 10^{-14}\,\text{cm}^2\,\text{s}^{-1}. \tag{24}$$

Alternatively the C–C bond at the R–O• site cleaves, leading to chain scission and the formation of carbonyl (HR=O) groups and the creation of a new R• radical site at rates of $10^3\,s^{-1}$:

$$\text{R–O•} \rightarrow \text{HR=O} + \text{R•}. \tag{25}$$

Surface radicals created by the further abstraction of H atoms from carbonyl groups (HR=O, •R=O) undergo addition reactions with OH resulting in acid groups (HO–R=O):

$$\text{HR=O} + \text{O} \rightarrow \text{•R=O} + \text{OH}, \qquad p = 0.04, \tag{26}$$

$$\text{HR=O} + \text{OH} \rightarrow \text{•R=O} + \text{H}_2\text{O} \qquad p = 0.4, \tag{27}$$

$$\text{•R=O} + \text{OH} \rightarrow \text{HO–R=O} \qquad p = 0.12. \tag{28}$$

Subsequent chain scission of the carbonyl radical •R=O leads to the formation of CO_2, a byproduct of surface treatment:

$$\text{•R=O} + \text{O} \rightarrow \text{RH} + \text{CO}_2 \qquad p = 0.1. \tag{29}$$

Termination steps include the recombination of alkyl radicals on the backbone by H and OH radicals:

$$\text{R•} + \text{H} \rightarrow \text{RH} \qquad p = 0.2, \tag{30}$$

$$\text{R•} + \text{OH} \rightarrow \text{R–OH} \qquad p = 0.2. \tag{31}$$

While ion bombardment is important to surface modification at low pressure where ion energies are tens to hundreds of eV [31], its role at atmospheric pressure is less clear since ions arrive at the surface at near thermal speeds. Ions might react similarly to their corresponding neutral states. For instance, O^+ and O_2^+ may react on the surface in a manner similar to O and O_2. Ions with non-reactive neutral analogues arriving at the polymer surface may still break bonds by virtue of the ionization potential worth of energy they bring to the surface and their inducing secondary electron emission from the surface. The secondary electron emission coefficient (γ) on dielectric surfaces due to ion bombardment at atmospheric pressure is estimated to be 10^{-3} to 10^{-2} [32]. We included ion reactions at the surface leading to the formation of surface radicals (R•) but given the short duration of pulses and the low fluxes of ions compared with neutrals, the contribution of ions to surface treatment is not expected to be significant. The reactions we included are

$$\text{RH} + \text{M}^+ \rightarrow \text{R•} + \text{H} - \text{M} \qquad p = 0.001. \tag{32}$$

UV and VUV photons emitted by the plasma can play an important role in surface kinetics and modifying polymer properties [33–35]. UV photons having energies of >4–5 eV can cleave C–C bonds on the surface forming alkyl (R•) sites. Skurat and Dorofeer [36] investigated photon-initiated reactions on polymer surfaces and determined that photochemistry proceeds via three major pathways. The dominant pathway is the elimination of H_2 from the hydrocarbon surface. This forms alkenes that subsequently react to form adjacent alkyl radical sites (–•RR•–). These sites have a higher probability of undergoing scission to form R• sites rather than recombining [33]. The sequence of events is

$$\text{RH} + h\nu \rightarrow \text{•R–CH–CH–R•} + \text{H}_2, \tag{33}$$

$$\text{•R–CH–CH–R•} \rightarrow \text{R=R}, \tag{34a}$$

$$\rightarrow \text{R•} + \text{R•}. \tag{34b}$$

The other two pathways for photon interactions result in forming R• radicals by breaking either the C–H bond releasing atomic hydrogen or causing C–C bond scission in the polypropylene backbone:

$$\text{RH} + h\nu \rightarrow \text{R•} + \text{H}, \tag{35a}$$

$$\rightarrow \text{R•} + \text{R•}. \tag{35b}$$

Skurat and Dorofeer estimated the probability for chain scission to be 4–5 times greater than H removal.

In this investigation, surface reactions resulting fluxes from UV and VUV photons emitted by excited gas species were included with an effective total quantum yield of 0.2 leading to the formation of alkyl (R•) sites [37]. Reaction probabilities for the constituent pathways in equations (33)–(35*a*) and (35*b*) were scaled accordingly as shown in table 1.

Surface radicals (R•) on adjacent PP backbones can react with each other to crosslink [5, 20, 38–40]. We included processes for surface radicals (R•) to locally crosslink with each other with an estimated rate of $10^{-15}\,cm^2\,s^{-1}$:

$$\text{•R–CH–CH–R•} + \text{R–H} \rightarrow \text{R=R}. \tag{36}$$

In the presence of reactive gas phase species which passivate surface radicals, the density of cross-linked sites is expected to be low.

4. Effect of gas composition and surface residence time

A schematic of the corona discharge device investigated here is shown in figure 1. The polymer sheet extends up to 5 cm on either side of a powered metal electrode embedded in dielectric with its tip exposed to the processing gas 2 mm from the polymer sheet. The 2D geometry uses Cartesian coordinates and so this configuration can be interpreted as a long linear corona bar into the plane of view. Gas enters from the left (initialized to have a uniform speed parallel to the surface on the left boundary) and exits to the right. The exit plane boundary condition is obtained by requiring the pressure to be constant and adjusting the total exit gas flow rate. When the sheet moves, it enters from the left and exits to the right. The discharge occurs between the powered electrode and the polypropylene (PP) sheet in contact with the lower grounded electrode. The pulse duration is typically short (<5 ns) and the pulse repetition frequency is 1–10 kHz. Up to a few tens of pulses and inter-pulse periods are simulated.

For the base case, we considered treatment of a non-moving polypropylene sheet in a repetitively pulsed $He/O_2/H_2O = 89/10/1$ discharge without forced gas flow. The applied voltage is −5 kV in a step function at 10 kHz. The densities of plasma species (electrons, positive ions, O atoms and OH radicals) at the time the electron avalanche reaches

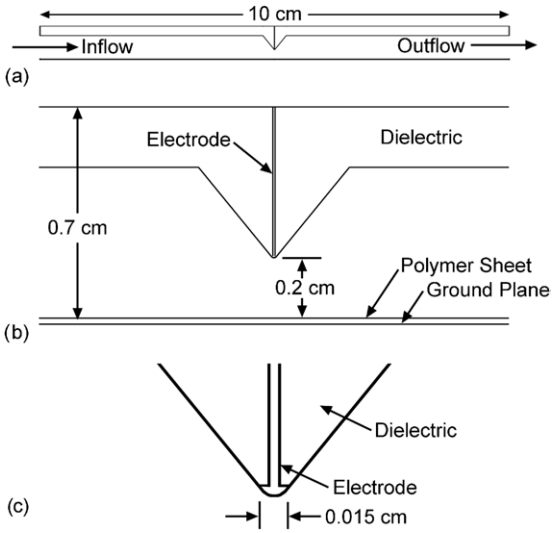

Figure 1. Schematic of the corona discharge. The upper electrode is powered and the polymer is placed on the lower grounded electrode separated by 2 mm and so functions as a dielectric barrier discharge. The computational domain is 10 cm with gas flowing in from the left and pumped to the right. The polymer sheet translates from the left end to right at speeds of hundreds of cm s^{-1}.

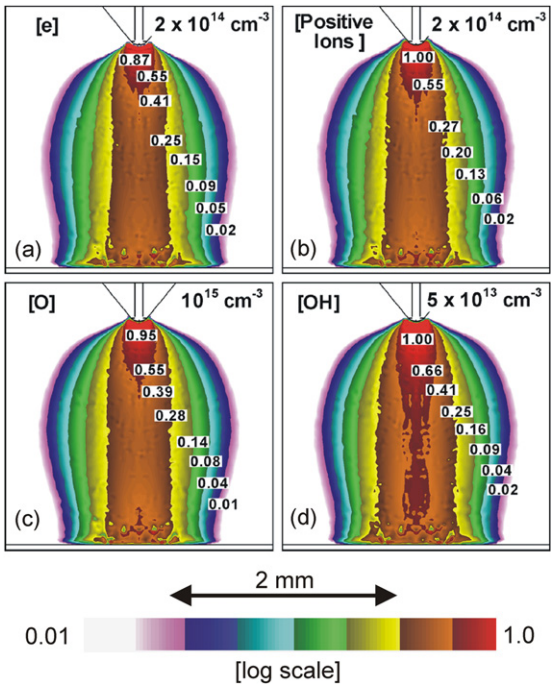

Figure 2. Species densities at the end of the first discharge for a $He/O_2/H_2O = 89/10/1$ mixture with a −5 kV pulse. (*a*) Electrons, (*b*) positive ions, (*c*) O atoms and (*d*) OH radicals. The maximum value is noted in each frame and contours are a 2-decade log scale. Contour labels are the fraction of the maximum. Radical densities of 10^{13}–10^{15} cm^{-3} are created during breakdown.

and begins to spread on the PP sheet (a few ns of propagation) for the first discharge pulse are shown in figure 2. Electron and ion densities of up to 10^{14} cm^{-3} occur in the high electric field region near the tip of the electrode, decreasing to a few times 10^{13} cm^{-3} above the PP. In this short time, little neutral chemistry occurs and so the densities of O (3×10^{14} cm^{-3})

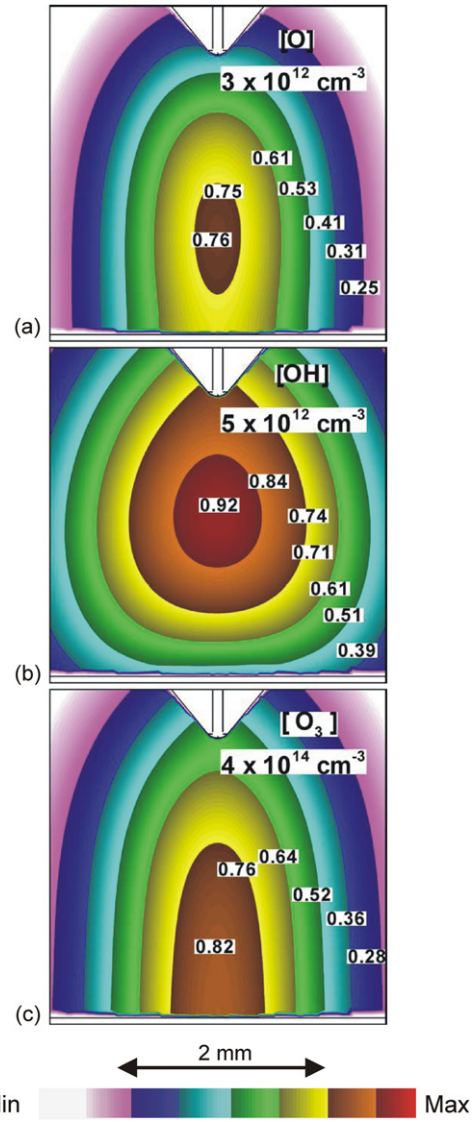

Figure 3. Densities of reactive gas phase species at the end of the inter-pulse period for a $He/O_2/H_2O = 89/10/1$ mixture with a −5 kV pulse. (*a*) O, (*b*) OH and (*c*) O_3. The maximum value is noted in each frame and contour labels are the fraction of the maximum. The bulk of O atoms are converted to O_3 by three body association reactions with O_2.

and OH (3×10^{12} cm^{-3}) above the PP sheet result largely from electron impact dissociation. Charging of the surface of the PP which removes voltage from the gap causes the discharge to extinguish. The plasma zone (that portion of the PP sheet directly treated by the plasma) is about 1 to 1.5 mm wide under the electrode.

The densities of O, OH and O_3 at the end of the first 100 μs inter-pulse period after the discharge are shown in figure 3. Recall that the reactivity probabilities of these species on the PP surface are a self-consistent outcome of the model. The slope of the density of the radicals into the surface is an indication of their reactivity. O atoms are generated by electron impact of O_2 during every discharge pulse. During the inter-pulse period, the peak density of O atoms is reduced by 2–3 orders of magnitude to 10^{12} cm^{-3} by the formation of O_3 while the density of O_3 increases to 10^{14} cm^{-3}. Neither O nor O_3

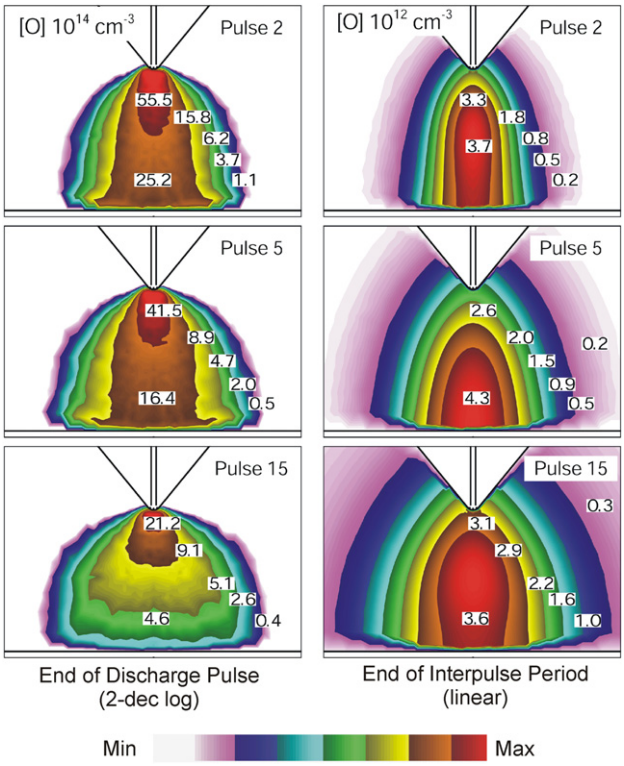

Figure 4. The density of O atoms at the end of pulses 2, 5 and 15 in the repetitive discharge for a $He/O_2/H_2O = 89/10/1$ mixture with a −5 kV pulse: (left) At the end of the discharge pulse and (right) at the end of the inter-pulse period.

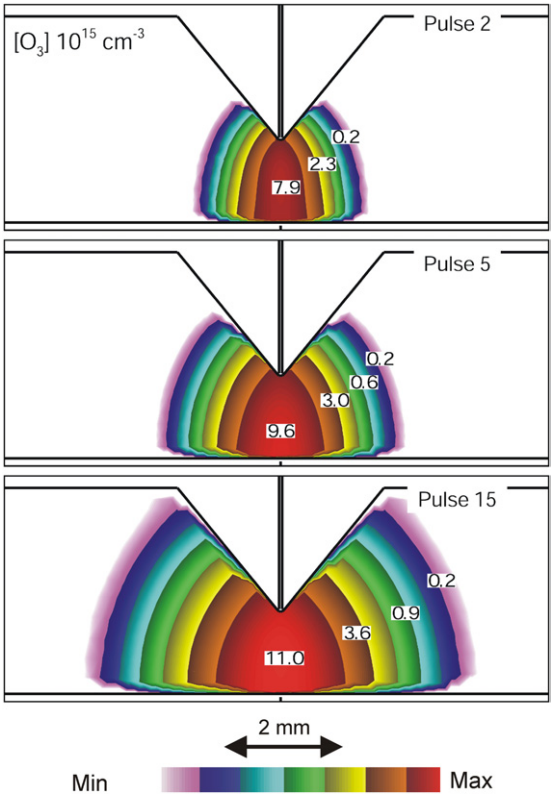

Figure 5. Density of O_3 at the end of the inter-pulse period for pulses 2, 5 and 15 pulses in the repetitive discharge for a $He/O_2/H_2O = 89/10/1$ mixture. O_3 accumulates pulse to pulse and diffuses from the discharge zone.

are particularly reactive with the surface. However a small reactivity coupled with their large densities results in their being influential in surface functionalization. For example, the large density of O_3 rapidly passivates alkyl (R•) sites in spite of the low reactivity for any single O_3 molecule. OH is consumed in reactions with O and O_3 in the gas phase while also being highly reactive with the surface. The end result is that the density of OH diminishes to 10^{12} cm^{-3} after the 100 μs inter-pulse period. Since there is no forced gas flow and the temperature rise during the single discharge pulse is only 10–20 K, convection is minimal and transport is dominated by diffusion.

The discharge is repetitively pulsed to increase or replenish the density of reactive gas phase radicals and enable a higher degree of functionalization. The densities of O atoms at the end of the 2nd, 5th and 15th discharge pulses and after their respective 100 μs inter-pulse periods are shown in figure 4. Since the O atoms are reactive in the gas phase, largely in making O_3, they are consumed during the inter-pulse period prior to the next discharge pulse and are replenished by electron impact dissociation by each discharge pulse. The maximum O density is roughly the same after each discharge pulse. The pulse-to-pulse variation in the O atom density at the end of the discharge pulse results from some amount of gas heating (a few tens of degrees) producing a small amount of rarefaction of the gas, a small change in background composition (principally increasing O_3 density) and some amount of residual charge left on the polymer. The spatial distribution does broaden with successive pulsing, which then decreases the O atom density at the surface of the PP.

The densities of the O atoms at the end of the inter-pulse period have maximum values of (2–5) × 10^{12} cm^{-3}, compared with their peak value at the end of the discharge pulse of 10^{15} cm^{-3}. The decrease is dominantly attributed to formation of O_3. Although there is some lateral diffusion, the O atoms are largely consumed at the sites of their production. Similarly, much of the OH generated during a given pulse is consumed during the inter-pulse period in reactions with O, O_3 and HO_2. In contrast, the peak density of O_3 increases on a pulse-to-pulse basis. For example, the densities of O_3 at the end of the 2nd, 5th and 15th inter-pulse periods are shown in figure 5. O_3 is relatively unreactive and accumulates from pulse-to-pulse with lateral diffusion broadening its extent. The density of O_3 reaches a maximum value in excess of 10^{16} cm^{-3} after 15 pulses.

Alkyl surface radicals (R•) are mainly created by H abstraction from the polymer backbone (RH) by reactions with O and OH radicals. This occurs dominantly within about 20 μs after the discharge pulse and in the immediate vicinity of the electrodes. The reactivities of O (primarily in the gas phase) and OH (both in the gas phase and on the surface) are sufficiently high such that their densities are depleted prior to diffusive transport extending their densities. As a result, H abstraction by these radicals is largely localized to being below the electrode. For example, the surface densities of alkyl sites are shown in figure 6(*a*) at the end of the discharge pulse and at the end of the inter-pulse period. (Although these values are shown for the first discharge pulse, the pattern

changes little for subsequent pulses.) The densities of peroxy (R–OO•) sites after the 1st, 5th, 10th and 20th inter-pulse periods are shown in figure 6(*b*). These densities are the sum of primary, secondary and tertiary sites. The alkyl sites are formed over tens of microseconds by abstraction reactions with O and OH formed in the immediate vicinity of the PP surface where the avalanche front encounters the surface. During the longer 100 μs inter-pulse periods, the alkyl sites are slowly converted to peroxy (R–OO•) groups by reactions with O_2. Although the probability of these reactions is small, the large density of O_2 succeeds in converting the majority of R• to R–OO• during the inter-pulse period. Since the peroxy sites are relatively unreactive, they tend to accumulate over many pulses. Similarly, a small fraction of alkyl radicals are converted into alkoxy groups (R–O•) by reactions with O_3 with densities that increase with the first 10 inter-pulse periods, as shown in figure 6(*c*), until coming into a steady state.

Given the reactivity of the precursor O and OH species and their limited diffusivity, more spatially extensive functionalization of the PP requires either forced gas flow or movement of the web. In this regard, the treatment of a moving polypropylene sheet by a repetitively pulsed $He/O_2/H_2O$ = 89/10/1 discharge without forced gas flow was examined. For example, the coverage of R–O• and R–OO• groups are shown in figure 7 for a polypropylene sheet moving from left to right at 400 cm s^{-1} after 5, 10 and 20 pulses. Alkyl (R•) radicals (figure 7(*a*)) are regenerated with every pulse at surface sites lying within a few mm of the corona tip due to renewed fluxes of O and OH. This leads to a spike in R• coverage following the pulse. As the polymer moves out of the discharge zone, these R• sites continue to react with O_2 to form peroxy (R–OO•), which increases their density downstream over many pulses. The coverage of peroxy groups approaches a steady state downstream of the discharge as the number of pulses increases and the alkyl sites are depleted. The modulation of the R–OO• coverage is a consequence of any given site on the polymer sheet moving outside the plasma zone where the R• formation peaks following a discharge pulse.

Although the alkyl sites are primarily produced by H abstraction from RH by O and OH, there is a also a continuing production of these sites. O_3 passivation of R• produces alkoxy sites (R–O•) which can abstract an H atom from a neighbouring RH thereby producing another alkyl site. Similarly, a peroxy (R–OO•) can also abstract H from a neighbouring RH site. This low level production of R• results in a tail of alkyl coverage that moves downstream with the web.

The relative coverage of alkoxy (R–O•), alcohol (R–OH) and carbonyl (R–C=O) compared to peroxy (R–OO•) groups is largely determined by the ratio of the flux of O_3 to O_2 during the inter-pulse period. Small ratios of O_3 to O_2 fluxes favour rapid passivation of alkyl sites to form peroxy groups. Large ratios of O_3 to O_2 fluxes favours formation of R–O• sites and initiates a sequence of reactions originating with alkyl and alkoxy sites, and terminating in carbonyl sites.

Carbonyl surface groups (including both HR=O and •R=O) are relatively stable products which result from a series of reactions beginning with production of an alkoxy site by O_3 (or O atom) passivating an alkyl site. Carbonyl groups are only slowly eliminated by erosion of the film producing

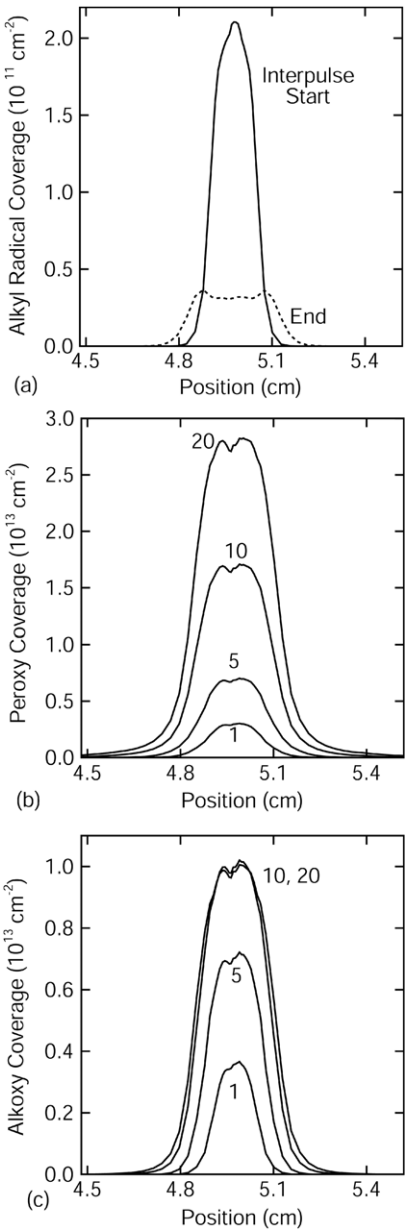

Figure 6. The coverage of surface groups formed on a static polymer surface during repetitive pulsing for a $He/O_2/H_2O$ = 89/10/1 mixture; (*a*) Alkyl (R–•) sites at the beginning and end of the inter-pulse period, (*b*) peroxy (R–OO•) sites at the end of the 1, 5, 10 and 20 inter-pulse periods and (*c*) alkoxy (R–O•) sites at the end of the 1, 5, 10 and 20 inter-pulse periods. Alkyl radicals are periodically regenerated and consumed in every pulse whereas peroxy sites accumulate from pulse to pulse. Alkoxy coverage achieves a steady state.

CO_2 or by conversion to alcohol groups (HO–R=O). One such sequence is

$$O + RH \rightarrow R\bullet + OH, \tag{37a}$$

$$R\bullet + O_3 \rightarrow R\text{–}O\bullet + O_2, \tag{37b}$$

$$R\bullet + O_2 \rightarrow R\text{–}OO\bullet, \tag{37c}$$

$$R\text{–}O\bullet + RH \rightarrow HR{=}O + R\bullet, \tag{37d}$$

$$HR{=}O + O \rightarrow \bullet R{=}O + OH \tag{37e}$$

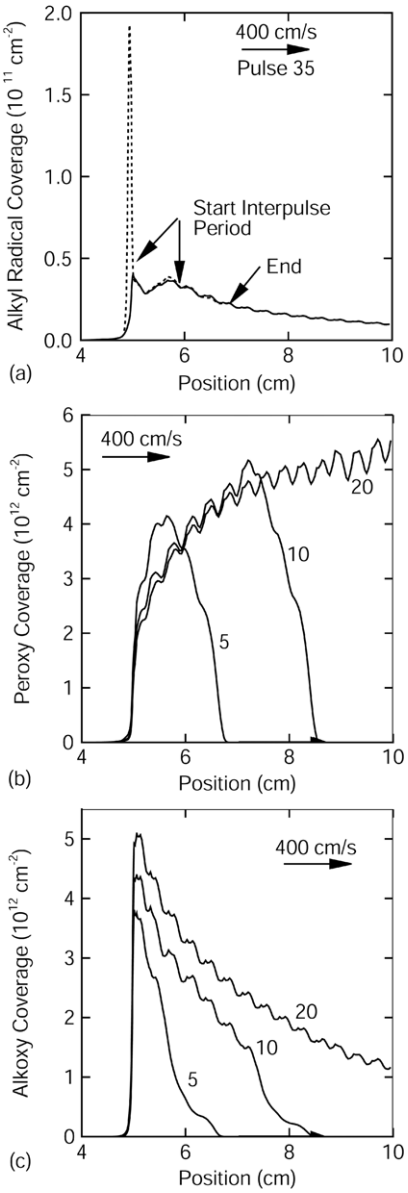

Figure 7. The coverage of surface sites for a $He/O_2/H_2O = 89/10/1$ mixture with film motion at 400 cm s^{-1} (from left to right) (*a*) Alkyl (R–•) sites at the beginning and end of the 35th inter-pulse period, (*b*) peroxy (R–OO•) sites at the end of the 5, 10 and 20 inter-pulse periods and (*c*) alkoxy (R–O•) sites at the end of the 5, 10 and 20 inter-pulse periods. Alkyl sites far from the discharge are regenerated by surface–surface reactions. Peroxy sites accumulate as the film moves whereas alkoxy sites are consumed largely by surface–surface reactions.

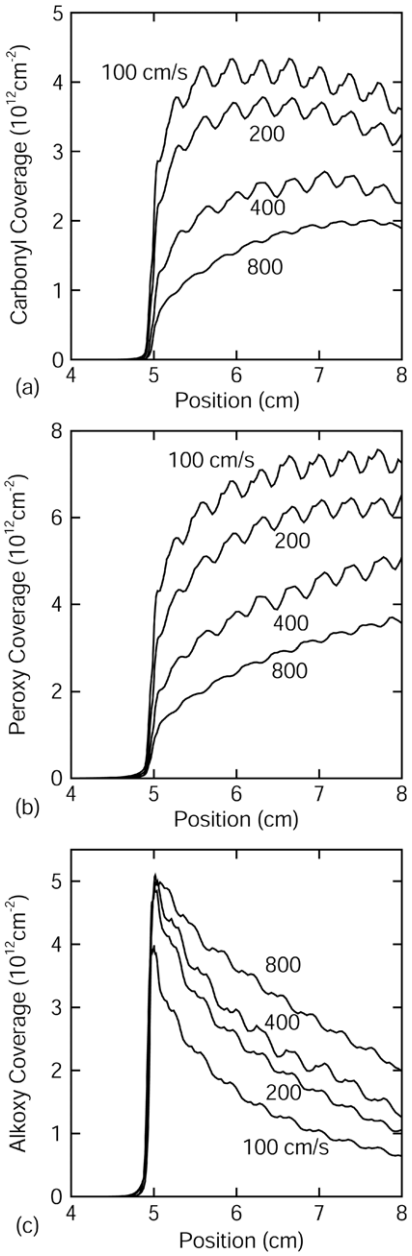

Figure 8. The effect of surface residence time on the coverage of (*a*) carbonyl (HR=O, •R=O), (*b*) peroxy (R–OO•) and (*c*) alkoxy (R–O•) groups in the absence of forced gas flow obtained by varying the speed of the film for a $He/O_2/H_2O = 89/10/1$ mixture. Larger residence times (lower film speeds) increase the coverage of carbonyl and peroxy groups while the coverage of alkoxy groups decreases.

$$HR{=}O + OH \rightarrow \bullet R{=}O + H_2O, \qquad (37f)$$

$$\bullet R{=}O + O \rightarrow RH + CO_2, \qquad (37g)$$

$$\bullet R{=}O + OH \rightarrow OH{-}R{=}OH. \qquad (37h)$$

The step which emphasizes the influence of the ratio of O_3 to O_2 fluxes on the subsequent reaction chain is the passivation of the alkyl site generating either alkoxy or peroxy groups (equations (37*b*) and (37*c*)). The latter (forming a peroxy) is largely a terminal step leading at best to hydroperoxy sites (R–OOH) by H abstraction from an adjacent RH on the backbone. The former (creating an alkyl) leads to carbonyl and alcohol formation.

The effect of surface residence time in the discharge zone on the coverage of carbonyl (R–C=O) and peroxy (R–OO•) groups is shown in figure 8 for different film speeds. The energy deposition per unit area was held constant by increasing the pulse repetition rate with the film speed. As such, the number of discharge pulses and the flux of O atoms a given site experiences is the same for each web speed. What differs is the length of time between pulses. At lower film speeds the time interval between pulses is longer and so the amount

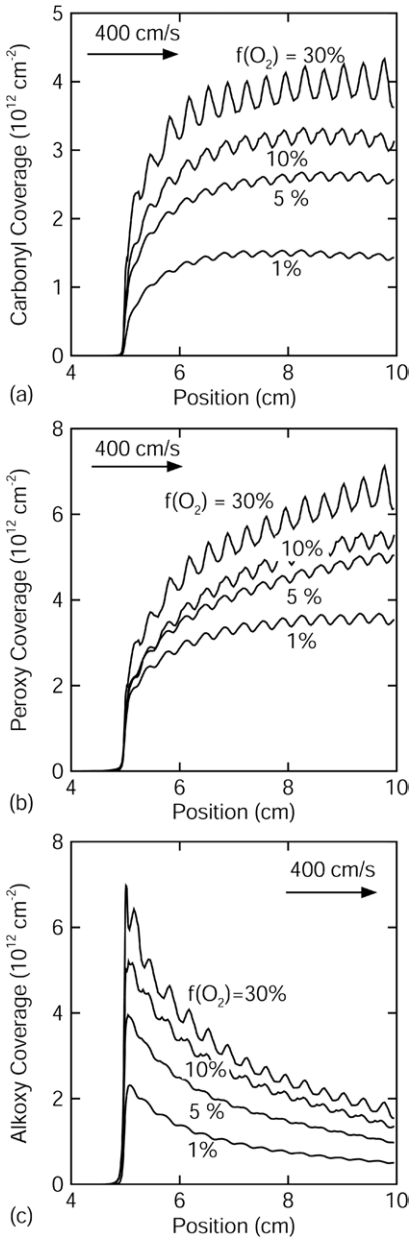

Figure 9. The effect of the fraction of oxygen, $f(O_2)$, in a $He/O_2/H_2O = 99 - x/x/1$ mixture on polymer surface treatment for constant film speed of 400 cm s^{-1} in the absence of forced gas flow. Higher degrees of surface treatment generally result from higher $f(O_2)$.

of inter-pulse processing, primarily by O_2, is larger. As a result a greater fraction of surface sites are saturated into peroxy groups in the discharge zone than into alkoxy groups by O_3. Alkoxy coverage decreases as these sites are converted into carbonyl groups downstream of the discharge zone, and so carbonyl coverage increases. New surface alkyl radicals are also created, which are then saturated predominantly into peroxy groups by O_2, so the peroxy coverage also increases downstream. The lower pulse frequency results in greater modulation of surface coverages at lower film speeds.

The competition between O_2 and O_3 fluxes in reacting with alkyl (R•) sites is demonstrated by varying the O_2 fraction $f(O_2)$ in the discharge. For example, peroxy and alkoxy coverages are shown in figure 9 while varying $f(O_2)$ from 1% to 30% for a web speed of 400 cm s^{-1}. Low values of $f(O_2)$ produce large fluxes of O-atoms and small fluxes of O_3. (Even at $f(O_2) = 1\%$, the flux of O_2, to the surface is large.) The total coverage of peroxy (R–OO•) sites, which are formed by the passivation of alkoxy (R•) sites by O_2, depends on the relative rates generation and consumption of R• sites. As $f(O_2)$ increases, the O atom flux during the discharge pulse increases which results in a higher rate of H abstraction from the polymer and increased production of alkyl (R•) sites. The R• sites formed on the surface in the discharge zone continue to react downstream and are passivated with O_2 to form peroxy (R–OO•). At constant film speed (and hence residence time), the degree of passivation by O_2 increases with $f(O_2)$ because there are both larger initial fluxes of O and larger fluxes of O_2.

The trends for alkoxy sites differ from that for peroxy groups when $f(O_2)$ is varied. In the discharge zone, increasing $f(O_2)$ increases the ratio of fluxes of O_3 to O_2 due to the higher rate of 3-body reactions. This increases the rate of formation of alkoxy (R–O•) sites by the passivation of R• (more of which are created by the larger O fluxes) by O_3. Since R–O• sites undergo scission reactions to form carbonyl groups at a finite rate and are only slowly regenerated due to the lack of O_3 downstream, they are consumed while carbonyl coverage increases as the polypropylene sheet moves downstream.

5. Effect of forced gas flow

The coverage of surface groups ultimately depends on the residence times of surface sites under the fluxes of gas phase radicals. Motion of the film is one way to influence these residence times and fluxes. Forced gas flow is another method. To investigate the influence of forced gas flow on polymer surface treatment the flow rate of the $He/O_2/H_2O$ mixture entering the computational domain was varied from 1 to 30 standard litres per minute (slpm) producing inlet speeds of 4 cm s^{-1} at 1 slpm to 120 cm s^{-1} at 30 slpm. Computationally, the fluid dynamics module of the model was first run to achieve a steady state at which time pulsing of the discharge commenced. For example, the initial flow field for a flow rate of 10 slpm is shown in figure 10 in the vicinity of the electrode. The flow speed increases in the discharge zone where the cross-section is the smallest. Recirculation occurs on the downstream side of the electrode structure.

The effects of forced gas flow on O atom generation during repetitive pulsing are shown in figure 11 for 30 slpm. (Compare with figure 4 for results without forced gas flow.) Here densities of O atoms at the end of the discharge pulse after 2, 5 and 10 pulses are shown. As without forced gas flow, the pulse-to-pulse variation in the O atom density is small, peaking at (2–3) $\times$ 10^{14} cm^{-3}. The O atoms are largely consumed by reactions during the first tens of μs of the inter-pulse period and during that time the forced gas motion is nominal.

The densities of O atoms, O_3 and OH at the end of the inter-pulse period after 2, 5 and 15 pulses are shown in figure 12 for a gas flow of 30 slpm. Although the vast majority of the O atoms are consumed by local kinetics in the discharge zone, a small density survives (on order of 10^{11} cm^{-3}) to be transported downstream during the inter-pulse period. The higher speed through the gap under the electrodes clears out the residual O

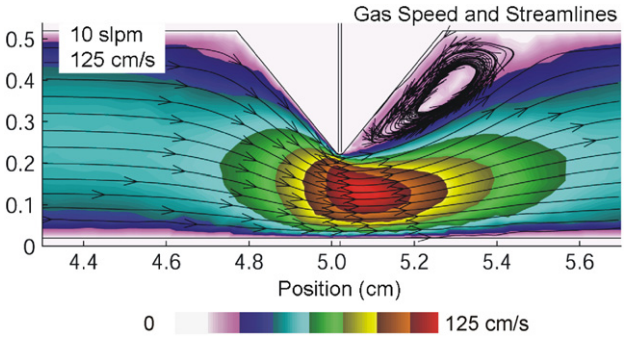

Figure 10. Flow streamlines with a forced gas flow of 10 slpm originating from the left. The contours are the speed of the gas with higher values near the electrode due to the smaller cross-sectional area. Recirculation occurs on the downstream side of the electrode.

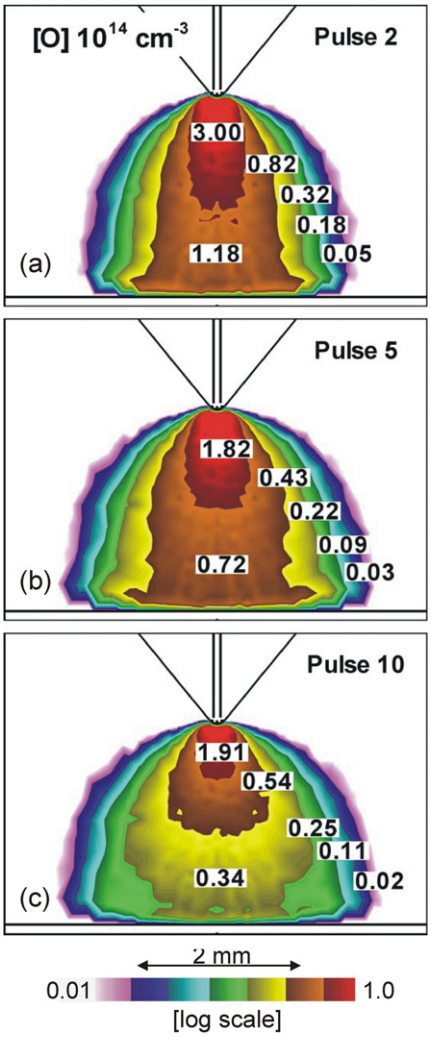

Figure 11. The density of O atoms at the end of successive discharge pulses for $He/O_2/H_2O = 89/10/1$ mixture with 30 slpm forced flow. (*a*) Pulse 2, (*b*) pulse 5 and (*c*) pulse 10. The peak density of O atoms decreases by a factor of 30% as the number of pulses increases.

atoms from the discharge zone creating a plume that is added to each pulse. Although the density of O atoms downstream is small, the inter-pulse period is long, and so some processing of the surface may result.

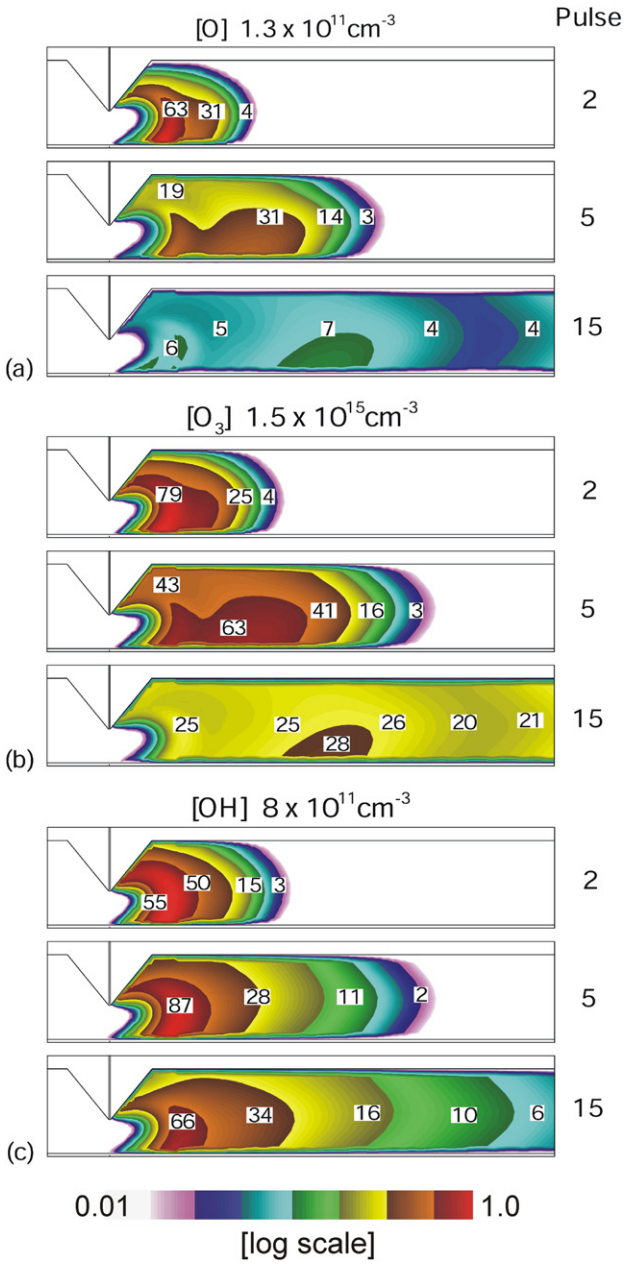

Figure 12. Reactive species densities at the end of the inter-pulse periods 2, 5 and 15 for a $He/O_2/H_2O = 89/10/1$ mixture with 30 slpm forced flow. (*a*) O atoms, (*b*) O_3 and (*c*) OH. The densities of O and OH are depleted downstream of the discharge after each pulse, creating a low density plume. O_3 accumulates in the discharge and produces a high density plume downstream. Most of the O_3 generated near the electrode is convected by gas flow downstream. The maximum density is shown at the top of each frame. The labels are percentages of the maximum value.

The behaviour of O_3 during repetitive pulsing with forced gas flow (figure 12(*b*)) is similar to that of the O atoms. The higher speed of the forced flow through the discharge zone clears out O_3 molecules following every pulse. Unlike O atoms, the O_3 are relatively unreactive and so accumulate in the discharge. The forced gas flow creates a plume of O_3 that extends progressively further downstream with each discharge pulse and inter-pulse period reaching densities above 10^{15} cm^{-3}.

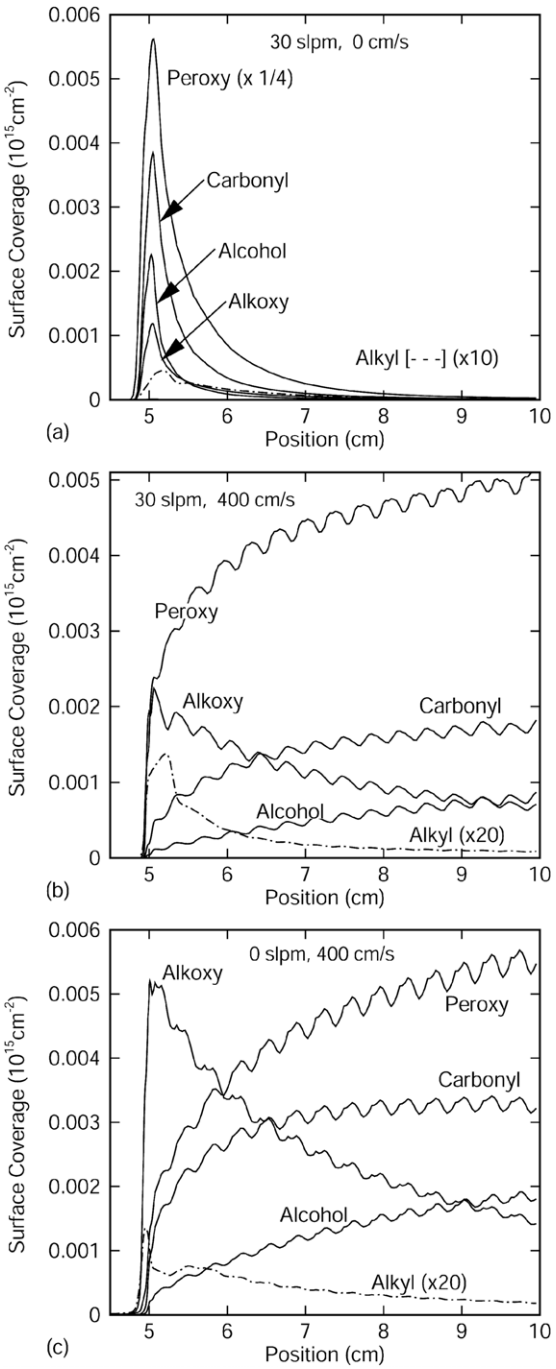

Figure 13. Coverage of surface groups for a He/O_2/H_2O = 89/10/1 mixture with different combinations of flow and movement of the film. (*a*) Flow of 30 slpm and static film, (*b*) flow of 30 slpm and film speed 400 cm s^{-1} and (*c*) no gas flow and film speed of 400 cm s^{-1}.

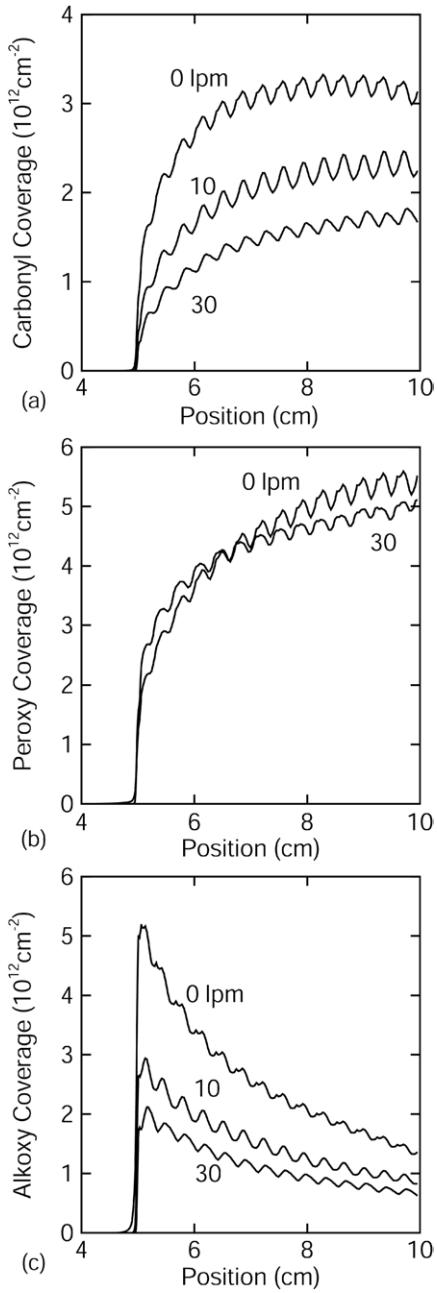

Figure 14. Comparison of the surface coverage of (*a*) carbonyl (HR=O, •R=O), (*b*) peroxy (R–OO•) and alkoxy (R–O•) groups on the polypropylene surface for a film speed of 400 cm s^{-1} for different amounts of gas flow. The relative flux of O_3 to O_2 in the discharge zone is decreased due to gas flow resulting in lower carbonyl and alkoxy coverage at higher flow rates.

The reactivity of OH is intermediate between O and O_3. On each discharge pulse, OH is created by electron impact dissociation, is entrained by the forced flow and creates a plume extending downstream (as shown in figure 12(*c*)). The OH radicals are consumed by reactions both in the gas phase and on the surface, and so the plume extends downstream with a progressively smaller density.

For a constant repetition rate of the discharge, by varying the volume of forced gas flow, f, and web speed, w, the fluxes of reactive species to the substrate can be controlled and so to some degree one can control the coverages of surface groups. The utility of this strategy is demonstrated by the results in figure 13 for the densities of alkyl (R•), alcohol (R–OH), alkoxy (R–O•) and peroxy (R–OO•) groups for: (*a*) f = 30 slpm, w = 0; (*b*) f = 30 slpm, w = 400 cm s^{-1} and (*c*) f = 0 and w = 400 cm s^{-1}. The discharge is repetitively pulsed at 1 kHz with a gas mixture of He/O_2/H_2O = 89/10/1.

With f = 30 slpm and w = 0 (figure 13(*a*)), the maximum coverages of surface groups occur under the

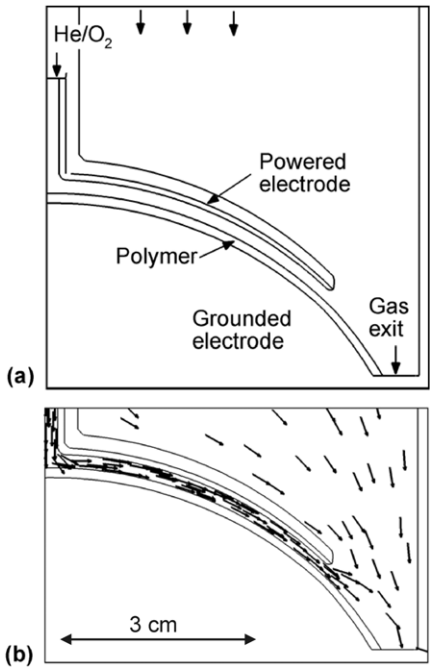

Figure 15. Polymer processing in a drum–shoe configuration that allows use of reactive inlet gases. (*a*) Schematic showing shoe-shaped powered electrodes at a distance of 2 mm from a grounded drum electrode. The polymer sheet rotates through the plasma zone. (*b*) Representative velocity flow field.

discharge. In the absence of web motion, the same surface receives refreshed fluxes of O and OH with every pulse, abstracting H from the polymer to create alkyl (R•) sites. The forced gas flow distributes O, OH and O_3 downstream, leading to significant alkyl and alkoxy formation downstream of the discharge zone. The large flux of OH radicals produced on each pulse above the same area where alkyl sites are continually being regenerated produces large coverages of alcohol and carbonyl sties.

With the addition of web motion ($f = 30$ slpm and $w = 400\,\mathrm{cm\,s^{-1}}$) R• sites are also continuously generated under the discharge zone, as shown in figure 13(*b*), and those heavily processed sites are translated downstream. Since the motion of the film is commensurate with the speed of the plume of reactive species, sites continue to receive the radical fluxes from the plume not unlike a motionless web without gas flow, albeit the fluxes are lower. With forced gas flow transporting O_3 downstream, the relative fraction of alkoxy (R–O•) sites remains high while the density of alkyl (R•) sites decreases by a factor of 6 due to reaction primarily with O_2. Surface–surface reactions redistribute functional groups as the film translates downstream. R–O• groups abstract H atoms from surrounding surface sites to form an increasing density of alcohol (R–OH) groups, while decreasing R–O• coverage. The density of R• sites decreases as they are saturated by O_2 to form R–OO• whose coverage increases downstream. The pulse to pulse modulation in O and OH densities that initiates the surface reactions as the film moves into and out of the discharge is reflected in the modulation of R–O• and R–OO•.

Surface coverages for $w = 400\,\mathrm{cm\,s^{-1}}$ but without forced gas flow are shown in figure 13(*c*). In the absence of forced gas flow, the initiating gas phase radicals are concentrated

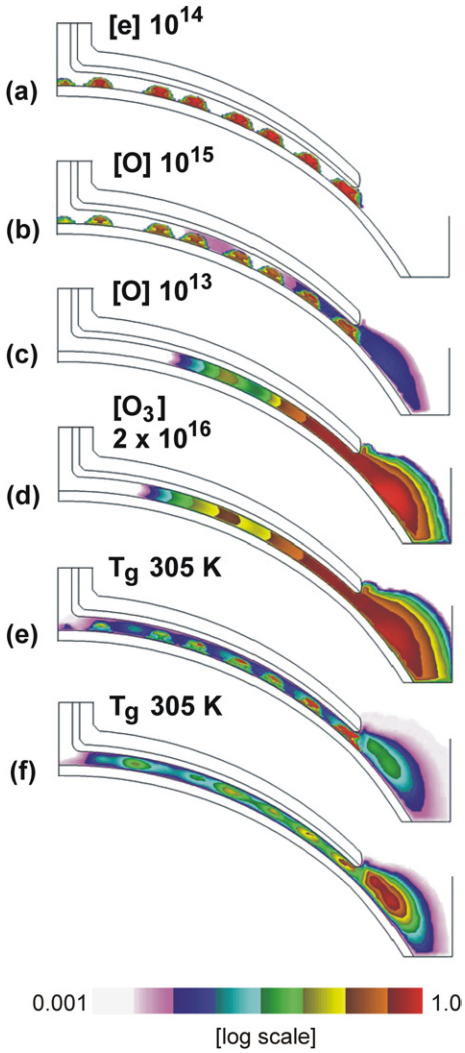

Figure 16. Plasma parameters for a $He/O_2 = 90/10$ gas mixture excited by alternate polarities at 1 kHz. (*a*) Electron density and (*b*) O atom density at end of a discharge pulse; (*c*) O atom and (*d*) O_3 density at end of an inter-pulse period; and gas temperature at end of (*e*) discharge pulse and (*f*) inter-pulse period.

in the discharge zone. With the accumulation of O_3 pulse to pulse, the ratio of O_3 to O_2 fluxes in the immediate vicinity of the discharge is high compared with other locations. As a result, most of the alkyl (R•) under the electrode are consumed in reactions with O_3 to form alkoxy (R–O•) sites. As the film moves out of the discharge region the formation of new sites by gas phase radicals diminishes and surface–surface reactions begin to dominate. New alkyl (R•) sites are regenerated downstream by hydrogen abstraction by R–O• to produce large alcohol (R–OH) and carbonyl coverages compared with other conditions. As the flux of other radicals diminishes downstream, R• are saturated with O_2 to form R–OO• groups.

The surface coverages of carbonyl (R–C=O), peroxy (R–OO•) and alkoxy (R–O•) groups for 0, 10 and 30 slpm flow with the polypropylene sheet moving at $400\,\mathrm{cm\,s^{-1}}$ are shown in figure 14. (Recall that for a moving web, the product coverages are those at the exit plane.) The largest density of alkoxy sites occurs under the discharge zone where the density

of alkyl sites peaks (by H abstraction by O and OH fluxes) followed by passivation by O and O_3. The R–O• sites are then depleted by chain scission reactions (creating carbonyl) and hydrogen abstraction (producing alcohol) as they move downstream. At higher gas flow rates, the coverage of R–O• decreases because convective transport of O_3 significantly reduces the ratio of fluxes of O_3 to O_2 in the discharge zone. The lower ratio of O_3/O_2 fluxes in the discharge zone allows a larger fraction of R• sites to be passivated by O_2. As carbonyl (R–C=O) sites are formed by reactions initiated by R–O•, the surface coverage of R–C=O decreases with gas flow as well.

6. Confined plasmas with multiple discharges

The use of reactive gases (such as NH_3) in open room-air environments requires more sophisticated gas injection and confinement systems [41, 42]. A schematic of one such apparatus is shown in figure 15 and consists of a grounded drum electrode separated by a gas gap of 1–2 mm from a powered cylindrical shell-shaped shoe electrode. The polymer sheet is placed on the drum electrode and is rotated through the discharge zone. Reactive gas mixtures are injected through the nozzle on the axis at slightly higher than atmospheric pressure. With forced gas flow through the narrow gap between the shoe-electrode and drum, a small overpressure occurs which prevents room air from back diffusing into the gap.

These geometries differ from the conventional corona discharge in that there are multiple discharges that occur along the length of the flow between the shoe-electrode and the drum. As such, fresh supplies of initiating radicals are produced above a surface site as it rotates with the drum. To illustrate these differences, the continuous treatment of polypropylene sheets was investigated using the geometry in figure 15. The diameter of the drum was 12 cm and the drum–electrode gap was 0.2 cm. A $He/O_2 = 90/10$ mixture was injected through the central nozzle at a flow rate of 100 slpm and pumped at the lower right corner, resulting in a gas velocity in the gap of about 915 cm s^{-1}. Although air would normally be the gas outside the electrode–drum gap, to simplify the computation, the exterior gas was also He/O_2. The exterior gas was injected at a flow rate of 100 slpm from the top surface. The resulting flow vectors are shown in figure 15(*b*). The upper electrode was powered at 15 kV with alternating polarities at a frequency of 1 kHz. Electrons were seeded at a finite number of randomly chosen locations in the discharge zone with every pulse to initiate the discharges. The polymer rotates through the plasma zone in a clockwise manner. In an actual device there would be a mirror image of the electrode on the other side of the mid-plane and so the polymer sheet would have been 'pretreated' prior to entering the computational domain shown in figure 15. To simplify the calculation, we assumed that the polymer sheet entering the computational domain from the left was untreated.

The electron and O atom densities at the end of the 6th discharge pulse are shown in figures 16(*a*) and (*b*). During any pulse, the peak electron density is about 10^{14} cm^{-3} and is generated adjacent to the momentary cathode (alternating between the top and bottom). Local sources of O atoms are produced at each discharge location during the pulse with peak densities of 10^{15} cm^{-3}. Gas heating raises temperatures by only about 5 K at the end of the discharge pulse, shown in figure 16(*e*). The narrow gap provides for rapid thermal conduction.

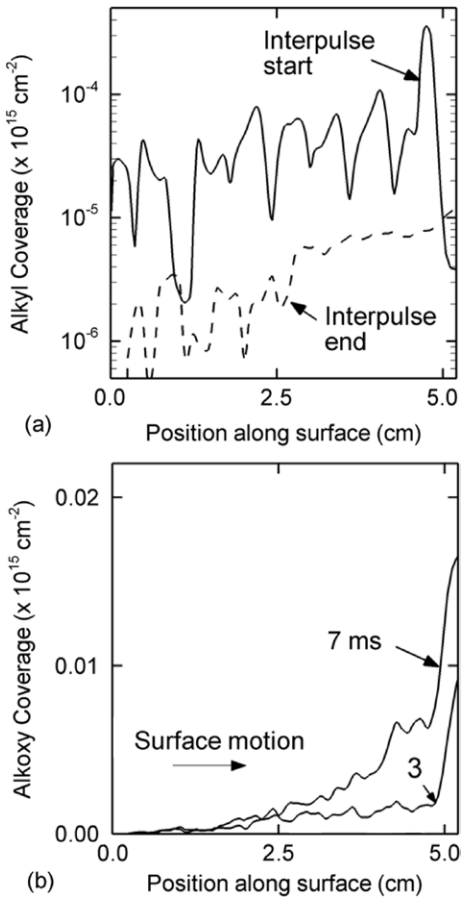

Figure 17. Surface properties as a function of position along the drum–shoe configuration: (*a*) alkyl (R•) and (*b*) alkoxy (R–O•) coverage. Alkyl coverage is high across the entire surface since it encounters renewed fluxes of abstracting O and OH radicals. Alkoxy coverage increases as the polymer exits the discharge due to stagnation of flow that increases densities of reactants.

By the end of the inter-pulse period convective flow transports some of O atoms downstream but the bulk of O is consumed to form O_3 and so these densities are greatly diminished from their peak, as shown in figure 16(*c*). O_3 accumulates around every discharge location following a pulse and is transported along the gap, shown in figure 16(*d*). The convective transport helps smooth out peaks of radical production across the sheet while maintaining a relatively high O_3 density within the discharge zone. A plume of O_3 extends beyond the electrode–drum gap and is eventually pumped away. The gas temperature in-between pulses changes little, shown in figure 16(*f*).

The resulting surface coverages of alkyl (R•) and alkoxy (R–O•) groups are shown in figure 17. The PP sheet repeatedly receives fresh fluxes of O and OH radicals at multiple (but random) locations as it moves through the discharge zone. At those locations, alkyl (R•) sites are regenerated by H abstraction reactions. At the end of the discharge pulse (beginning of the inter-pulse period) the alkyl coverage is large along the entire sheet, markedly different from the conventional corona discharge where the alkyl sites peak only directly under the bar

electrode. The R• sites are quickly saturated during the inter-pulse period. It is possible that some locations on the polymer surface may receive higher radical fluxes than others due to the randomness of the discharges. Nevertheless, convective transport does smooth out spatial gradients to a large extent. As a consequence, the alkoxy coverage monotonically and generally smoothly increases along the direction of motion. The continuous renewal of R• sites and the high O_3 density increases the fraction R–O• coverage as the polymer exits.

7. Concluding remarks

Control of the process variables gas flow, gas composition and film speed during continuous treatment of polymer sheets may enable the tailoring of the composition of surface functional groups. During treatment of polypropylene in repetitively pulsed $He/O_2/H_2O$ discharges, the initiating radicals O and OH are regenerated during every discharge pulse and generally consumed during the inter-pulse period by gas phase and surface reactions. Treatment of the film by O and OH is dominantly in the direct vicinity of the discharge. The O atoms are largely consumed to form O_3 and the longer-lived O_3 accumulates over many pulses. Gas flow transports longer lived species over a larger surface area creating a plume downstream which extends surface treatment. The motion of the web translates the surface out of the discharge zone and determines the time the surface receives large fluxes of the initiating radicals (O and OH) under the discharge. Since surface–surface reactions occur independent of the fluxes of gas phase radicals, the surface continues to evolve between discharge pulses and as it translates downstream. The plume of gas phase radicals produced by gas flow can intercept these reaction pathways.

The management of the flux of initiating radicals and of the ratio of O_3/O_2 fluxes in large part determines the final surface functionality. For example, the drum–shoe electrode configuration having multiple discharges along its length provides renewed radical fluxes as the surface passes through each discharge. At the same time, a high ratio of O_3/O_2 fluxes is also maintained throughout the discharge region. The end result is a film dominated by alkoxy groups.

Acknowledgments

This work was supported by the National Science Foundation (CTS-0520368) and 3M Inc. The authors thank Dr Mark Strobel of 3M for his advice and guidance.

References

[1] Chan C-M 1994 *Polymer Surface Modification and Characterization* (New York: Hanser/Gardner)
[2] Jones V, Strobel M and Prokosch M J 2005 *Plasma Process. Polym.* **2** 547
[3] Abdel-Salam M, Mizuno A and Shimizu K 1997 *J. Phys. D: Appl. Phys.* **30** 864
[4] Akishev Y, Grushin M, Napartovich A and Trushkin N 2002 *Plasmas Polym.* **7** 261
[5] Strobel M, Lyons C S and Mittal K L (ed) 1994 *Plasma Surface Modification of Polymers* (Zeist, The Netherlands: VSP Press)
[6] O'Hare L-A, Leadley S and Parbhoo B 2002 *Surf. Int. Anal.* **33** 335
[7] Kwon O J, Tang S, Myung S W, Lu N and Choi H S 2005 *Surf. Coat. Technol.* **192** 1
[8] Borcia G, Anderson C A and Brown N M D 2003 *Plasma Sources Sci. Technol.* **12** 335
[9] Kogelschatz U 2003 *Plasma Chem. Plasma Process.* **23** 1
[10] Wang M C and Kunhardt E E 1990 *Phys. Rev.* A **42** 2366
[11] Vitello P A, Penetrante B M and Bardsley J N 1994 *Phys. Rev.* E **49** 5574
[12] Kulikovsky A A 2000 *J. Phys. D: Appl. Phys.* **33** 1514
[13] Eliasson B, Egli W and Kogelschatz U 1994 *Pure Appl. Chem.* **66** 1275
[14] Chen J and Davidson J H 2002 *Plasma Chem. Plasma Process.* **22** 495
[15] Carman R and Mildren R P 2003 *J. Phys. D: Appl. Phys.* **36** 19
[16] Oda A, Sugawara H, Sakai Y and Akashi H 2000 *J. Phys. D: Appl. Phys.* **33** 1507
[17] Eichwald O, Guntoro N A, Yousfi M and Benhenni M 2002 *J. Phys. D: Appl. Phys.* **35** 439
[18] Martin A R, Shawcross J T and Whitehead J C 2004 *J. Phys. D: Appl. Phys.* **37** 42
[19] Clark D T and Dilks A 1977 *J. Polym. Sci. Polym. Chem. Edn.* **15** 2321
[20] Clark D T and Dilks A 1979 *J. Polym. Sci. Polym. Chem. Edn.* **17** 957
[21] Normand F, Grainer A, Leprince P, Marec J, Shi M K and Clouet F 1995 *Plasma Chem. Plasma Process.* **15** 173
[22] Dorai R and Kushner M J 2003 *J. Phys. D: Appl. Phys.* **36** 666
[23] Liu C, Brown N M D and Meenan B J 2005 *Surf. Sci.* **575** 273
[24] Wang C and He X 2006 *Surf. Coat. Technol.* **201** 3377
[25] Arakoni R, Stafford D S, Babaeva N Y and Kushner M J 2005 *J. Appl. Phys.* **98** 073304
[26] Chorin A J 1997 *J. Comput. Phys.* **135** 118
[27] Rahman M M and Siikonen T 2001 *Numer. Heat Transfer* B **40** 391
[28] Kushner M J 2005 *J. Phys. D: Appl. Phys.* **38** 1633
[29] Zhang D and Kushner M J 2000 *J. Appl. Phys.* **87** 1060
[30] Bhoj A N and Kushner M J 2006 *J. Phys. D: Appl. Phys.* **39** 1594
[31] Hong J, Truica-Marasescu F, Martinu L and Wertheimer M R 2002 *Plasmas Polym.* **7** 245
[32] Tochikubo F, Chiba T and Watanabe T 1999 *Japan. J. Appl. Phys.* **38** 5244
[33] Wertheimer M R, Fozza A C and Hollander A 1999 *Nucl. Instrum. Methods Phys. Res.* B **151** 65
[34] Wilken R, Hollander A and Behnisch J 1999 *Surf. Coat. Technol.* **116–119** 991
[35] Truica-Marasescu F, Jedrzejowski P and Wertheimer M R 2004 *Plasma Process. Polymer* **1** 153
[36] Skurat V E and Dorofeev Y I 1994 *Die Ang. Makromol. Chem.* **216** 205
[37] Kuvaldina E V, Rybkin V V, Titov V A, Shikova T G and Shutov D A 2004 *High Energy Chem.* **38** 411
[38] P-Epaillard F, Vallon S and Drevillon B 1997 *Macromol. Chem. Phys.* **198** 2439
[39] P-Epaillard F, Brosse J C and Falher T 1997 *Macromolecules* **30** 4415
[40] Hansen R H and Schonhorn H 1966 *J. Polym. Sci.* B **4** 203
[41] Meiners S, Salge J G H, Prinz E and Foerster F 1998 *Surf. Coat. Technol.* **98** 1121
[42] Wagner H-E, Brandenburg R, Kozlov K V, Sonnenfeld A, Michel P and Behnke J F 2003 *Vacuum* **71** 417